

Electronic structure of copper studied by electron momentum spectroscopyM. Vos,^{1,*} A. S. Kheifets,¹ C. Bowles,¹ C. Chen,¹ E. Weigold,¹ and F. Aryasetiawan²¹*Atomic and Molecular Physics Laboratories, Research School of Physical Sciences and Engineering,
Australian National University, Canberra ACT 0200, Australia*²*Research Institute for Computational Sciences, AIST, Tsukuba Central 2, Umezono 1-1-1, Tsukuba Ibaraki 305-8568, Japan*

(Received 16 June 2004; published 10 November 2004)

We present electron momentum spectroscopy measurements of the electronic structure of copper single crystals. Generally, good agreement was found with the band dispersion as measured by photoemission. The energy-resolved momentum densities are quite anisotropic. Observed diffraction effects can be disentangled in first order, and the experiment compares well to calculated momentum density. Deviations of the Fermi surface from spherical symmetry are resolved by this scattering experiment. Many-body effects cause lifetime broadening of the quasiparticle peak and a smooth tail extending to higher binding energies, but no clear satellite structures were found.

DOI: 10.1103/PhysRevB.70.205111

PACS number(s): 71.20.Be, 79.20.Kz, 71.10.-w

I. INTRODUCTION

Copper is probably the best studied metal. Our knowledge of the properties of electrons in Cu is extensive. For example, copper has been the testing ground for techniques mapping the Fermi surface (de Haas–van Alphen effect¹), measuring the band dispersion (photoemission²) and the determination of momentum densities using positron annihilation.^{3,4} Generally, the electronic structure of copper is supposed to be well understood, and these measurements are often seen as a test of the spectroscopy, rather than as a test of the understanding of Cu.

One of the oldest and conceptually simplest probes of the electronic structure is Compton scattering.⁵ It is thus somewhat surprising that state-of-the-art Compton measurements show a considerable difference between the calculated and measured Compton profiles.⁶ The measured profiles were too low in intensity for low momentum values, and the calculated anisotropy exceeded the measured anisotropy significantly. These differences can be explained only in part as electron correlation effects.⁷ This suggests that standard density functional theory (DFT) does not describe the momentum densities well.

Our knowledge of the electron dispersion is based on a large number of angle-resolved photoemission (ARPES) studies. Comparing the ARPES results with theory based on standard DFT calculations,^{8,9} one finds generally that the measured total bandwidth is somewhat smaller than the calculated one (8.6 eV relative to the calculated value of 9.3 eV²). In addition, the agreement for the actual position and the width of the *d* band is less than perfect. The binding energy of the top of the *d* band is underestimated (calculated binding energy is too small by about 0.5 eV) and the calculated *d* band width is too large (calculated width exceeds the experimental width by 0.3 eV). Recently, band dispersion calculations including self-energy effects have become available.^{10–12} Here the self-energy is calculated in terms of the Green's function *G* and a dynamically screened Coulomb interaction *W* (*GW* approximation). In the calculations from Marini *et al.*¹¹ based on a pseudopotential approach, much improved agreement with experiment was found. However,

all-electron, *GW* calculations show much smaller self-energy corrections.¹⁰

Here we present electron momentum spectroscopy (EMS) data of single-crystal copper films. We describe to what extent EMS can reveal the many known properties of electrons in copper (dispersion, shape of the Fermi surface, momentum densities). We explore if the energy-resolved momentum densities can shed light on the deviations found in the Compton profiles and if many-body corrections are required to get a good description of dispersion. As EMS measures densities as well as dispersion, it is, in principle, a more complete test of theory than either Compton scattering (measuring a projection of the momentum density) or photoemission (measuring dispersion). A truly quantitative interpretation of EMS data is more difficult than Compton scattering data as the incoming and outgoing electrons interact strongly with the target, and hence multiple scattering effects are non-negligible. Dispersion measurements by EMS can suffer from limited energy resolution (≈ 1 eV) in cases wherein lifetime broadening is negligible, but this high-energy technique has the advantage that it is not significantly affected by deviations of the final state from that of a free electron, and it does not have any problems associated with the loss of information of k_{\perp} at the surface. Thus, EMS has a combination of qualities that gives it a unique window on the electronic structure of materials. Here we compare the EMS results of copper with results obtained from other techniques.

An EMS experiment is an (*e*, 2*e*) experiment in the high-energy limit where the plane-wave impulse approximation is valid.¹³ An incoming electron with an accurately known momentum and energy has a binary collision with a target electron. This electron is ejected and both scattered and ejected electron are analyzed for energy and momentum. Using the laws of energy and momentum conservation, we can determine the energy and momentum transferred to the target, as

$$\varepsilon = E_0 - E_1 - E_2, \quad (1)$$

$$\mathbf{q} = \mathbf{k}_0 - \mathbf{k}_1 - \mathbf{k}_2, \quad (2)$$

with the subscripts 0,1,2 referring to the incident and emitted electrons, respectively. The frequency of occurrence of a co-

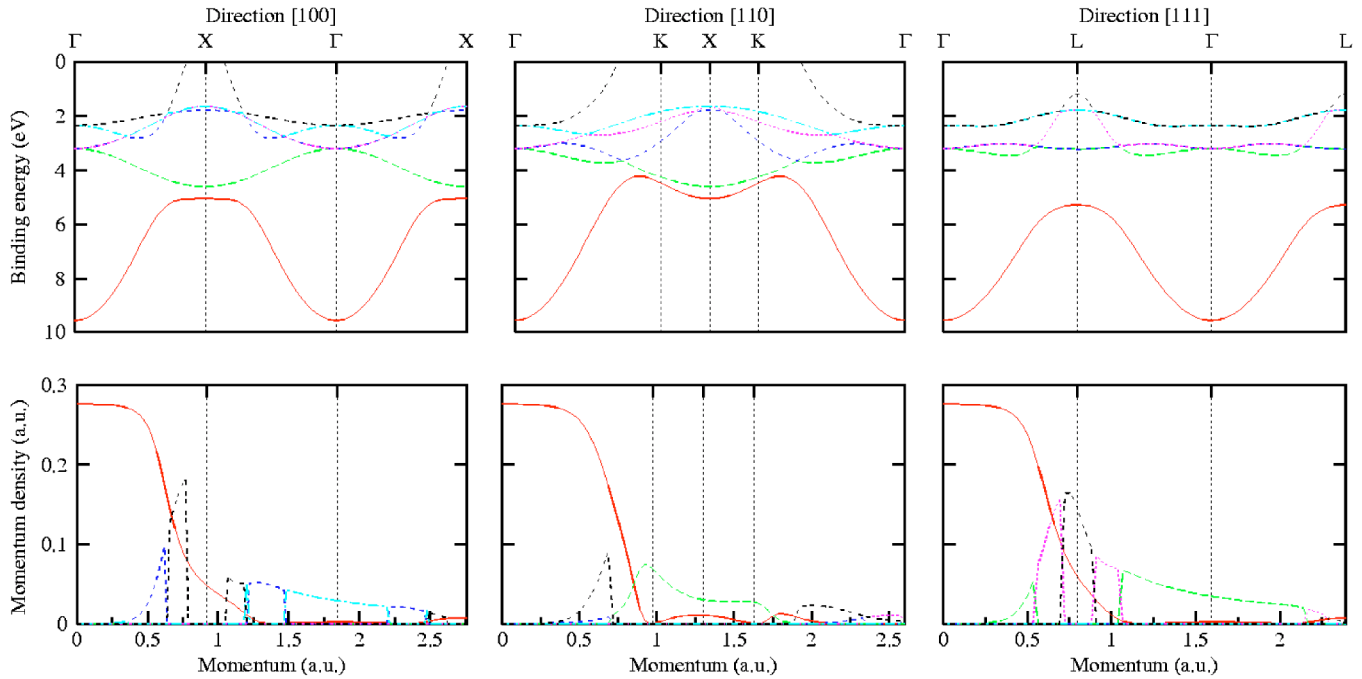


FIG. 1. (Color online) The dispersion as calculated by the full-potential linear tin-muffin orbital method along the three major symmetry directions (upper panel). The momentum densities, split up for the different bands, is shown in the lower three panels; the linestyle of each momentum density curve is the same as that of the dispersion of the corresponding band.

incident event with a certain $(\varepsilon, \mathbf{q})$ combination is proportional to the magnitude of the spectral momentum density (SMD) at that $(\varepsilon, \mathbf{q})$ combination. Within a one-electron picture this can be rephrased. In that case the measured intensity at $(\varepsilon, \mathbf{q})$ is simply proportional to the probability that a target electron has a binding energy, momentum combination $(\varepsilon, -\mathbf{q})$

In these one-electron theories, the electronic structure is traditionally plotted as a band structure, i.e., energy versus crystal momentum \mathbf{q}_c , and the wave function is presented for that reduced momentum by Bloch functions $\psi^j(\mathbf{r}) = \sum_{\mathbf{G}} C_{\mathbf{G}}^j e^{-i(\mathbf{q}_c + \mathbf{G}) \cdot \mathbf{r}}$ with j the band index. Dispersion along symmetry directions is plotted in Fig. 1, as well as their occupation $|C_{\mathbf{G}}^j|^2(\mathbf{q})$. These calculations were based on the full potential linear muffin-tin orbital (FP-LMTO) theory,¹⁴ but similar results are obtained using the atomic sphere approximation LMTO.¹⁵ For a given \mathbf{q}_c , the top panel gives the band energies, whereas from the bottom panel we find the value of $|C_{\mathbf{G}}^j|^2$ at $\mathbf{q} = \mathbf{q}_c + \mathbf{G}$.

These experiments are done at high kinetic energies (tens of keV for all electrons involved). Hence, the approximation that these electrons can be described as plane waves becomes a very good one. In addition, any refraction at the entrance or exit surface can be shown to be negligibly small. Hence, many of the problems associated with the interpretation of angular-resolved photoemission (final state wave functions, k_{\perp} not conserved) are not present in EMS. The experimental estimate of the spectral function is obtained directly by the data acquisition software, without the computer being fed any information about the sample under investigation.

II. EXPERIMENTAL DETAILS

The spectrometer details are described extensively elsewhere.^{16–18} Here we restrict ourselves to a brief description of the spectrometer and some details specific to the copper samples. In our spectrometer (Fig. 2,) a well collimated high-energy electron beam with an energy E_0 of 50 keV, and a corresponding momentum \mathbf{k}_0 of 62.1 atomic units (1 a.u. of momentum corresponds to $\approx 1.89 \text{ \AA}^{-1}$), impinges on a thin target. Electrons scattered over an angle of 44.3° are detected in coincidence at energies near 25 keV ($k_{1,2} = 44.3$ a.u.). The exact energy of both detected electrons ($E_{1,2}$) and their azimuthal angle $\phi_{1,2}$ (and hence momentum $\mathbf{k}_{1,2}$) are determined. In our experiment the scattering geometry is chosen in such a way ($\theta = 44.3^\circ$) that recoil momentum of detected coincidence events $\mathbf{k}_0 - \mathbf{k}_1 - \mathbf{k}_2$ is directed, in good approximation, along the y direction ($q_x \approx q_z \approx 0$) and its magnitude is proportional to $\phi_1 - \phi_2$.

Some bands do not contribute density according to Fig. 1. This does not mean that these bands are unoccupied or that they cannot be measured by EMS. In this paper we present measurements of the energy-resolved momentum density along high-symmetry directions; i.e., lines in momentum space that contain zero momentum. If we change the scattering angle (of either one or both of the detectors) away from $\theta = 44.3^\circ$ we would obtain the momentum density along a line (in momentum space) that does not contain zero momentum. By changing the scattering angle in such a way that the measurement line shifts by a reciprocal lattice vector, the dispersion will remain unchanged, but the contribution of different bands to the observed intensity will be completely different, and the “invisible bands” may contribute. For the

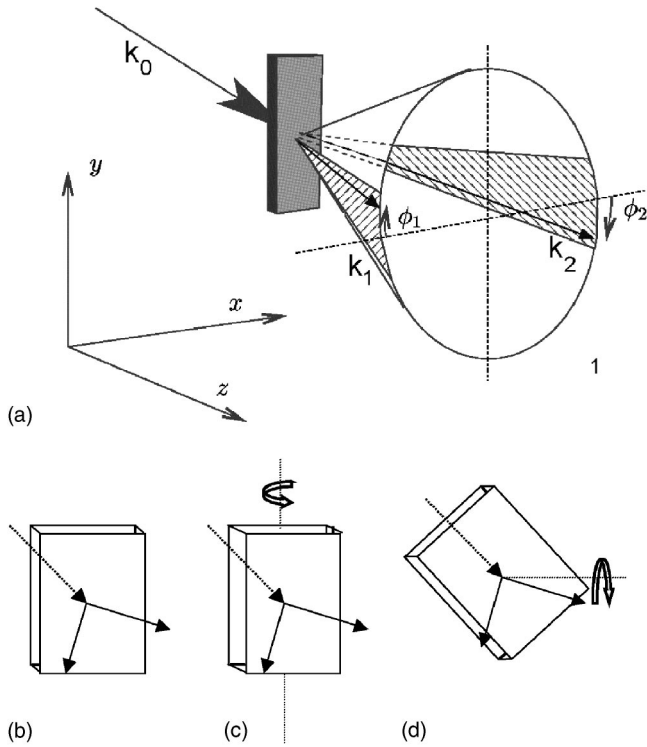


FIG. 2. In (a) we show a schematic representation of the measurement. Incoming electrons (momentum k_0) impinge on a thin film and two analyzers, measuring simultaneously a series of azimuthal angles $\phi_{1,2}$ and energies $E_{1,2}$, select coincident pairs of emerging electrons with momenta k_1 and k_2 . The sample is indicated as a block with a surface normal along the $\langle 0, \bar{1}, 1 \rangle$ direction, the edges oriented along the $\langle 0, 1, 1 \rangle$ and $\langle 1, 0, 0 \rangle$ crystal directions. In (b) we measure the SMD along the $\langle 1, 0, 0 \rangle$ direction, and the incoming beam is directed along $\langle 0, \bar{1}, 1 \rangle$. The outgoing electrons are moving close to $\langle 0, 1, 0 \rangle$ and $\langle 0, 0, 1 \rangle$ directions. In (c) we measure the SMD along the same direction, but the crystal has been rotated along the y axis by 10° moving the incoming and outgoing electrons away from high-symmetry directions. In (d) the crystal was rotated along the $\langle 0, \bar{1}, 1 \rangle$ axis by 54.4° and the SMD along a $\langle 1, 1, 1 \rangle$ direction is measured. A rotation over 90° results in a measurement along $\langle 0, 1, 1 \rangle$.

case of silicon, the effects of changing the scattering angle have been described elsewhere.¹⁸

The single-crystal Cu film was grown on a $\langle 110 \rangle$ NaCl crystal at the University of Aarhus. The film thickness was 100 nm. The NaCl was dissolved in deionized water and the copper was transferred to the sample holder (a shim containing an array of 0.2-mm-diameter holes) as a freestanding film, with the copper covering many holes. Subsequently the film was sputter-thinned until it became completely transparent and the film broke for some of the covered holes. No attempt was made to anneal the sputtered samples, and defects will be present in the surface layer. Measurements were subsequently done on an adjacent hole that was completely covered by an intact thin Cu film. The film orientation was initially judged from the known crystal orientation of NaCl substrate on which it was grown, and subsequently checked by transmission electron diffraction. Misalignments were

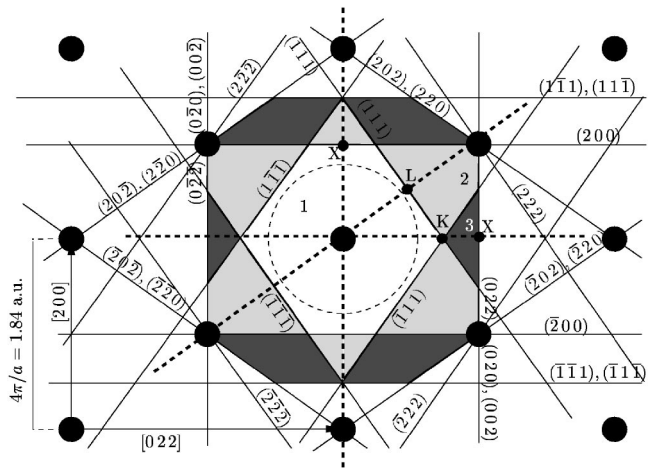


FIG. 3. A cut through reciprocal space (with $p_{\langle 0, \bar{1}, 1 \rangle} = 0$) showing the first three Brillouin zones. The free electron Fermi sphere for one electron per unit cell is drawn as a dashed circle. The three directions along which the spectral momentum density was determined are indicated by dashed lines. Some of the special points customarily used to describe high-symmetry points of the Brillouin zone are indicated as well.

corrected by rotating the sample *in situ*.

The measurements were done with the spectrometer y -axis oriented along the $\langle 100 \rangle$, $\langle 111 \rangle$, and $\langle 011 \rangle$ directions (the dashed lines in Fig. 3), as explained in Fig. 2. For a polycrystalline sample, elastic scattering causes a smooth background in the observed momentum densities, but for a single crystal, diffraction of the incoming and/or outgoing electrons can cause additional sharp structures in the measured spectral momentum distribution. For the case of silicon these effects have been discussed extensively.¹⁹

As the incoming momentum and outgoing momenta are rather large, the diffraction condition $2k_j \cdot G_i + G_i^2 = 0$ requires that G_i is almost perpendicular to k_j ($j=0,1,2$). Inspection of the incoming and outgoing electron trajectories with respect to the crystal lattice will point to the reciprocal lattice vectors that are most likely to contribute. Often one can minimize diffraction by rotating the sample around the spectrometer's y axis [see Fig. 2(c)]. This does not affect the direction along which the SMD is determined, but for a suitable rotation angle will reduce the number of possible reciprocal lattice vectors that contribute to diffraction.

III. ANISOTROPY IN SINGLE-CRYSTAL FILMS

A. General remarks

By rotating a film along its $\langle 0, \bar{1}, 1 \rangle$ surface normal, we can align the spectrometer y axis (the measurement direction) with the $\langle 1, 0, 0 \rangle$, $\langle 1, 1, 1 \rangle$, and $\langle 0, 1, 1 \rangle$ directions (see Fig. 2). As we can rotate the sample *in situ* only over a limited range, we prepared three different samples, each close to a desired orientation. At zero transferred momentum, the shapes of the spectra for all three samples were very similar (see Fig. 4). A broad peak stands out clearly at 9 eV binding energy, and corresponds to electrons emitted from the bottom

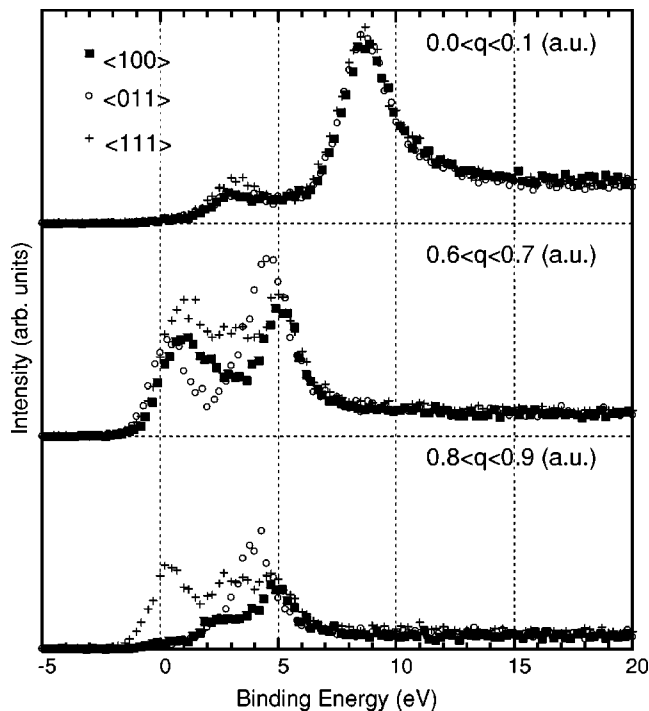


FIG. 4. Spectra of crystals with different orientations for selected momentum intervals. The three measurements for different orientations were normalized for the spectra near zero momentum.

of the band. A significant part of the intensity at larger binding energies (e.g., near 20 eV) is due to multiple scattering, i.e., ejection of a valence band electron plus additional energy loss of the outgoing and/or incoming electrons (e.g., by plasmon excitations). The relative probability of these multiple scattering events increases with sample thickness. These zero momentum spectra were scaled to equal height at the maximum intensity. Some differences observed at zero momentum near 3 eV binding energy have to be attributed to different amounts of diffraction, but the background at large energy loss, caused by inelastic scattering, is surprisingly similar. The similar intensity at high binding energies is somewhat surprising as some variation in thickness between the samples is expected and, as a result, there should be different amounts of inelastic scattering.

As (the q_y component of) the transferred momentum is increased, the main peak disperses to smaller binding energy, but up to 0.4 a.u. the spectra obtained for the three different orientations remain very similar. Large differences are observed, however, between 0.6 and 1 a.u., a range of momentum values for which the bands are close to Brillouin zone boundaries. A few examples are shown in Fig. 4. Thus, in spite of the presence of (sputtering-induced) defects in the surface layer, we resolve clearly the anisotropy of the electronic structure. This is expected due to the bulk sensitivity of this high-energy electron spectroscopy.

The measurements along different symmetry directions all contain spectra for zero momentum. By scaling the measurements in such a way that all three zero momentum spectra have equal maximum height, we obtain the same intensity scale for all momenta along the three measured directions. Thus, in the study of momentum densities, only a single

normalization factor between theory and experiment should be able to describe all three sets of data.

A few remarks should be made about the alignment of the energy scales of the different measurements. It must be remembered that we are doing spectroscopy with an energy resolution of 1 eV, while the energies of the particles involved are 50 and 25 keV. The point at which the sample intersects the electron beam can change by up to 0.3 mm from sample to sample. This causes a noticeable shift (0.5 eV) in the position corresponding to the Fermi level. Hence, we have to align slightly the energy scales of the different measurements.

With some care it is possible to establish the Fermi level position with an accuracy of about 0.25 eV, a value significantly smaller than the actual energy resolution (1 eV). The actual energy of a spectrum taken at k_f that corresponds to the Fermi level (e.g., maximum of the peak or 50% of maximum at the leading edge) depends on the ratio of momentum and energy resolution, as discussed for a free electron band structure by Vos *et al.*²⁰ Similar considerations are used here. For the $\langle 1,0,0 \rangle$ and $\langle 0,1,1 \rangle$ the zero momentum spectra align, using the zero energy level deduced from the spectra taken at the Fermi momentum. For the $\langle 1,1,1 \rangle$ direction the band does not intersect the Fermi level. Hence, we aligned the zero momentum spectra of the $\langle 1,1,1 \rangle$ direction with those of the $\langle 1,0,0 \rangle$ and $\langle 0,1,1 \rangle$ measurement. We infer in this way that for the $\langle 1,1,1 \rangle$ direction the band appears to approach the Fermi level to within 0.25 eV. This is in reasonable agreement with several calculations (e.g., Ref. 11). However, the well known Cu(1,1,1) surface state is at a binding energy of ≈ 0.4 eV, which dictates a minimum binding energy at the L point of 0.4 eV. The somewhat smaller observed binding energy at the L point is due at least in part to the finite momentum resolution. Indeed, a substantially larger value of 0.85 eV was derived from in photoemission experiments;²¹ this value seems to be at the upper limit of values consistent with the present data.

B. Dispersion

Obviously the anisotropy of the electronic structure is well resolved in the measurements. In order to determine the dispersion in a systematic way, the peak positions were determined by curve fitting, including a background subtraction. As the peaks stand well clear from the background, most fits are very straightforward. The dispersion obtained is plotted in Fig. 5 for all three directions. A rather complete mapping of the band structure is obtained by EMS, most occupied bands have a peak that can be tracked over most of the momentum range with significant occupation density. Some bands can be followed well outside the range with significant occupation. This is a clear sign that diffraction of the incoming and/or outgoing electrons is significant. Diffraction causes a shift in the momentum balance equation by a reciprocal lattice vector. As the band structure (in the repeated zone scheme) is periodic in the reciprocal lattice, the intensity associated with diffracted probe electrons coincides again with the band structure. For comparison with theory it is more useful to plot the spectra at the special points of the

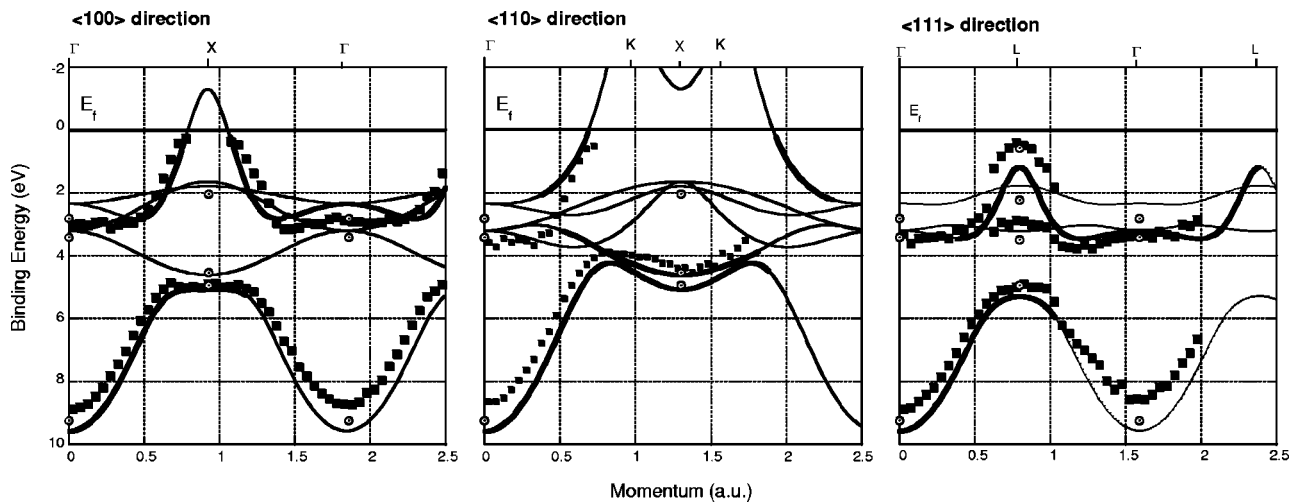


FIG. 5. A comparison of the measured dispersion with that obtained by a FP-LMTO calculation. The open circles are the band energies corrected for self-energy effects, as calculated by Marini *et al.*¹¹ Without diffraction, significant intensity is expected only for the part of the band structure that is indicated by a thick line.

Brillouin zones. This is done in Fig. 6, together with the calculated positions. Note that spectra taken at different locations in momentum space, but all corresponding to Γ points, have different intensity distributions, but similar peak positions.

Figure 5 also shows the band structure as obtained from a DFT calculation.¹⁴ Agreement between the standard DFT band structure calculation and the experiment is less than perfect. However, the disagreement observed is completely in line with state-of-the-art photoemission results.²² The total observed band width is slightly larger than the calculated band width, but the observed d -band width is smaller than the calculated one. Recently these discrepancies have been explained in terms of self-energy effects.¹¹

The total width of the occupied band structure was found to be 8.75(0.4) eV. This is in good agreement with the photoemission data [8.60(0.05) eV], as given in the compilation of experimental data by Courths and Hüfner,² but somewhat smaller than the value obtained by density functional theory (9.3 eV).¹⁴

C. Fermi surface anisotropy

The Fermi surface of copper is well known. De Haas–van Alphen measurements have shown that along the $\langle 100 \rangle$ and $\langle 110 \rangle$ directions the magnitudes of k_f are 0.827 and 0.743 a.u., respectively. Along the $\langle 111 \rangle$ direction the Fermi surface touches the Brillouin zone boundary. Photoemission

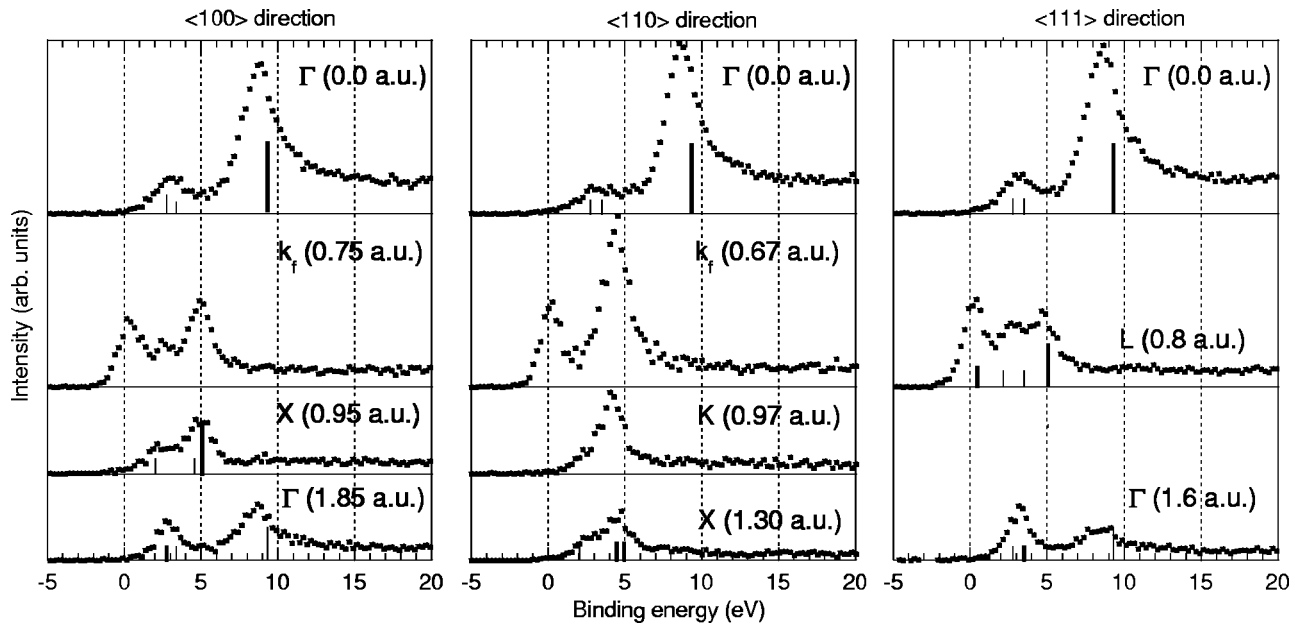


FIG. 6. The measured spectra near several special points. Energies as calculated by Marini *et al.*¹¹ are indicated by bars. Without diffraction, intensity is only expected at the thick bars.

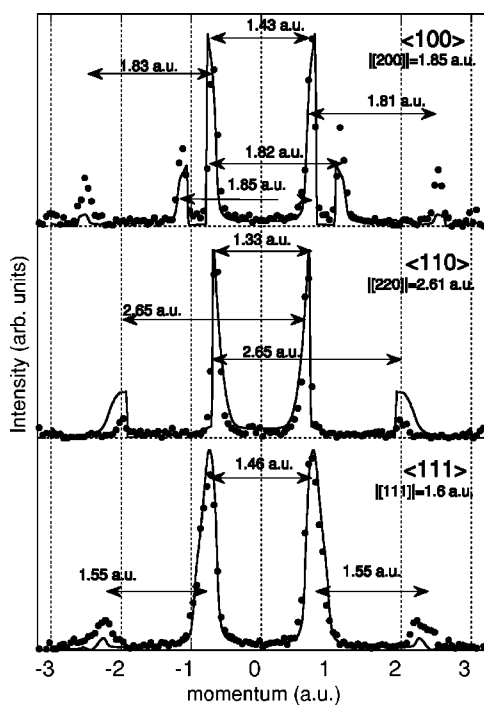


FIG. 7. The momentum density integrated over a 1-eV-wide window near the Fermi level for the three main symmetry directions. The theory is integrated over a 2-eV-wide window.

has been used with some success to map the Fermi surface of copper (see Nielsen *et al.*,²³ and references therein), but the interpretation of these data is rather involved due to the uncertainties in k_{\perp} .

For EMS measurements, information about the Fermi surface can be obtained by plotting the measured intensity near 0 eV binding energy. These measured momentum densities are shown in Fig. 7 for the different symmetry directions. In order to improve the statistics, the experiment was integrated over a 1 eV window near E_f . The separation of the peaks is shown in this drawing as well. Besides the main peaks, smaller peaks are seen at higher momentum. These smaller peaks are separated from the main peak by a reciprocal lattice vector, and are due at least in part to diffraction. The separation of the main peaks corresponding to the Fermi sphere diameter is larger in the $\langle 100 \rangle$ direction compared to the $\langle 110 \rangle$ direction. Using a simple interpretation that the separation of these two peaks is $2k_f$, one obtains values of 0.72 and 0.67 a.u. respectively, which are somewhat smaller than those obtained by the de Haas-van Alphen technique. However, due to finite energy resolution and finite energy integration window, states at a slightly larger binding energy and hence with a somewhat smaller magnitude in momentum contribute as well. These effects were simulated semiquantitatively for the case of a free electron solid,²⁰ and deviations of the order observed here are in line with our momentum and energy resolution. The theoretical line was obtained by integrating the theory over the outermost 2 eV, rather than exactly at 0 eV binding energy. The 2 eV window is in part due to the finite energy resolution (1 eV) and in part due to the integration width of the experiment (1 eV). At first sight one would expect that an energy window of $\sqrt{2}$ eV rather

than 2 eV would describe the experiment. In practice the 2 eV line shapes compared somewhat better. This is probably due to some additional broadening due to finite momentum resolution in the direction perpendicular to q_y (i.e., in the theory $q_x=q_z=0$, whereas in the experiment these components have a distribution around zero, due to finite momentum resolution). The shape of the theoretical distribution is in good agreement with the experiment. The experimental estimate of the anisotropy (0.05 a.u.) is somewhat smaller than the anisotropy of the de Haas-van Alphen measurements (0.084 a.u.) but this difference is smaller than the momentum resolution of the experiment (0.1 a.u.).

As along the $\langle 111 \rangle$ direction the separation of the maximum of the band from E_f is less than our energy resolution, we also see two peaks for this direction. These peaks have a considerably broader momentum distribution as they are derived from a band extremum rather than from a Fermi level crossing. One would judge from the dispersion alone that the two main peaks are separated by the length of a $\langle 111 \rangle$ reciprocal lattice vector (1.6 a.u.), whereas the separation of the maxima is observed at 1.46 a.u. Again the difference can be explained by the sharp decline in momentum density with increasing momentum in combination with finite energy resolution (see Fig. 1).

Of more concern is the deviation of the measured intensity at high momentum magnitudes in the $\langle 110 \rangle$ case. Here the theory predicts a significant intensity component near 2 a.u., whereas the experiment only shows a minor contribution. Part of the measured intensity could be related to diffraction, hence the experiment suggests strongly that the theoretical intensity near 2 a.u. is too large. As the high-momentum component is an indication of d character in the wave function at the Fermi surface, this could be rephrased by stating that the experiment indicates a wave function of mainly s character at the Fermi surface, whereas the theory predicts more d character.

The $\langle 100 \rangle$ and $\langle 111 \rangle$ orientations show significant amount of diffraction (at all binding energies, see Sec. III E). Hence the observed intensities at high-momentum components, which significantly exceed the calculated ones, are mainly due to diffraction, and an analysis similar to the $\langle 110 \rangle$ case (which displays surprisingly little diffraction) is not possible.

D. Inelastic multiple scattering

It is clear from the examples in Fig. 4 that the measured intensities extend beyond the energy range predicted by the band structure calculations. This intensity has two causes. Firstly, the incoming and outgoing electrons may lose energy due to inelastic scattering (e.g., plasmon excitations, interband transitions). This results in too large a binding energy being associated with an (e, 2e) event. This we refer to as inelastic multiple scattering. Its contribution increases with increasing film thickness, as the changes of inelastic scattering increases with path length of the electrons inside the film.

The second cause of intensity at high binding energy is due to many-body effects of the electronic structure. The sudden removal of an electron in an (e, 2e) event can lead to excitations of the electron gas. These excitations are often

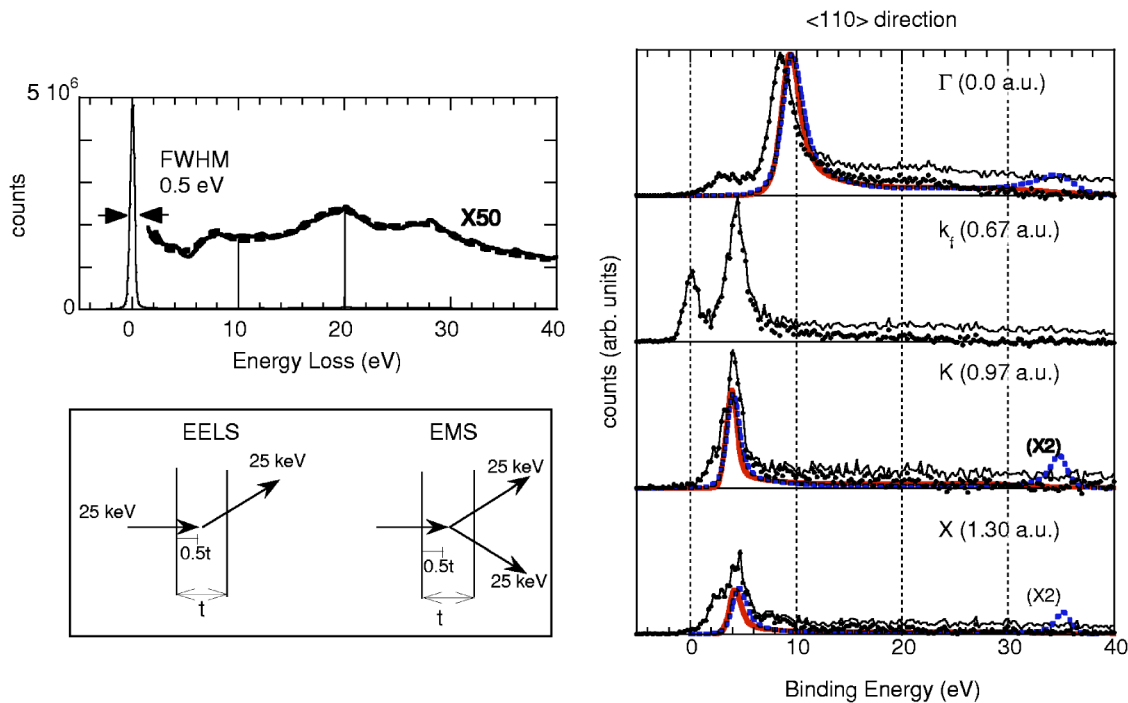


FIG. 8. (Color-online) In the top-left panel we show an energy loss spectrum, taken with 25-keV incoming electrons. The full line represents the experimental data, the dotted line an empirical fit used in the deconvolution procedure. In the bottom-left panel we compare the trajectories in this EELS experiment with those of the EMS experiment. The measured energy loss distribution is used to deconvolute the EMS data for inelastic scattering. The result of this procedure is shown in the right panel for the measurement along the $\langle 110 \rangle$ direction. The raw data (thin lines) are compared after deconvolution (dots) with GW calculation (blue, dotted lines) and cumulant expansion calculations (thick, red line)

referred to as intrinsic plasmons. Calculations of the spectral function based on many-body theory should be able to reproduce these effects. The probability of the excitation of intrinsic plasmons is independent of film thickness. In this paragraph we try to disentangle both contributions and compare the measured spectral function, corrected for inelastic scattering, with many-body calculations. For x-ray photoelectron spectroscopy (XPS), such theories have been developed by Tougaard (see, e.g., Ref. 24). However, the EMS data are richer than XPS data, allowing for momentum-resolved studies of the intrinsic satellites of the valence band.

The correction for inelastic scattering is based on the measured electron energy loss (EELS) spectrum of the same film. For this purpose the incoming energy is lowered to approximately 25 keV, and the energy loss distribution is determined in the spectrometer (Fig. 8, top left panel). As the analyzer is at the same angle as in the (e, 2e) measurement, all detected electrons have been deflected over an angle near 44.3° by elastic scattering from the potential of a nucleus. From this measurement we can determine the ratio of events at zero energy loss and at nonzero energy loss; i.e., the probability of electrons suffering inelastic scattering. The “average” EELS event will happen at thickness $0.5t$, where t is the sample thickness, and the same applies to the (e, 2e) events (see Fig. 8, bottom left panel). We can compare the effective path length of both experiments. We do this for the average EELS event and the average (e, 2e) event happening at $0.5t$. This is only an approximation. The probability that an inelastic excitation occurs along the incoming beam is approxi-

mately two times smaller for the average (e, 2e) event compared to the EELS experiment, as the incoming energy is twice as high in the (e, 2e) case. The probability that an inelastic event happens in the (e, 2e) case for the outgoing electrons is twice as high, as now two trajectories are involved. The average outgoing trajectory has a length of $0.5t/\cos(44.3^\circ)$. Based on these considerations, we assume that an energy loss event is 1.4 times more likely in the (e, 2e) experiment compared to the EELS experiment.

We subtract the effect of inelastic multiple scattering from the EMS data in the following way: We start at the Fermi level, where $E=0$ and the observed intensity is $I(E=0)$. This intensity $I(0)$ is due to “true” events; i.e., they are *not* contaminated by inelastic multiple scattering. Some intensity $I(E+\Delta)$ is due to (e, 2e) events at the Fermi level ($E=0$) in combination with an energy loss event of magnitude Δ [e.g., the incoming electron created a plasmon with energy Δ before the (e, 2e) event at $E=0$ occurred]. In the energy loss spectra, with the area of the zero loss peak normalized to 1, we find an intensity of y at an energy loss value Δ . Thus, in the (e, 2e) experiment we can expect, at a binding energy $E+\Delta$, a contribution $1.4yI(0)$ from events at $E=0$. This amount is subtracted from the observed intensity.

After correcting all intensities at higher binding energy for the contribution of $I(0)$, we consider the next energy bin. It could only have been contaminated from (e, 2e) events at the Fermi level plus small energy loss. However, this has been subtracted in the previous iteration. Hence, we can consider its modified intensity as being free from contamination

due to inelastic scattering. Now we use this modified intensity to correct intensity at larger binding energy from contamination from (e, 2e) events in the second bin. This process continues until the high binding energy limit of the spectrum is reached. This deconvolution procedure depends on the measured loss spectrum only, without adjustable parameters. It is expected to work well for films of thickness less or equal to one inelastic mean free path at 25 keV.

The results for the $\langle 110 \rangle$ direction are shown in the right panel of Fig. 8, and compared (for the high symmetry points Γ , K , and X) with calculations based either on the GW approximation or the cumulant expansion scheme.²⁵ The $\langle 110 \rangle$ direction was chosen as it is least affected by diffraction effects (see Sec. III E). In the calculation we focused on the peak shape, and no attempt was made to obtain the self-energy corrections to the band dispersion (requiring calculations on a dense grid in \mathbf{k} -space, rather than several special points). Therefore, we fixed the theoretical band width using the LMTO value. In the GW calculation the quasiparticle peak shape is well described, but it predicts a clear intrinsic-plasmon-type satellite (near 35 eV binding energy) not seen in the experiment. For the cumulant expansion calculation the agreement in peak shape between theory and deconvoluted experiment is reasonable. Both experiment and cumulant expansion theory display a rather featureless tail extending to higher energies.

E. Diffraction and its influence on the measured momentum densities

In Fig. 7 we see not just peaks at $\pm k_f$, but also peaks that are shifted by a reciprocal lattice vector. There are two reasons, that, in the experiment, intensity appears at more than one momentum value.

In the first place, the valence electrons in solids are Bloch waves: $\psi_{e,q_e}(r) = \sum_G C_G e^{i(\mathbf{G} + \mathbf{q}_e) \cdot \mathbf{r}}$. For an infinitely thin crystal, EMS measures the energy-resolved momentum densities and hence determines the contribution $|C_G|^2$ of the different plane wave components to the Bloch function.

Secondly, for a crystal of finite thickness the incoming, scattered, and ejected electrons interact with the crystal lattice. The theory of the influence of diffraction is described extensively elsewhere.^{26,27} Here we give a simplified account necessary to understand the extent of validity of the data analysis procedure used. We can write the wave function of the incoming and outgoing electrons $\psi_{0,1,2}$ as a set of plane waves with amplitude changing with depth: $\psi_{0,1,2} = \sum_G C_{0,1,2}^G(z) e^{i(\mathbf{k}_{0,1,2} + \mathbf{G}) \cdot \mathbf{r}}$. The boundary conditions are that at the entrance surface $C_0^{G=(0,0,0)} = 1$ and all other $C_0^G = 0$. Similarly at the exit surface $C_{1,2}^{G=(0,0,0)} = 1$ and all other $C_{1,2}^G = 0$.

To keep the language simple we restrict ourselves now to a noninteracting electron system. We measure a certain one-electron orbital with wave function in momentum space $\phi(\mathbf{q}_e)$. Without diffraction, the measured intensity I observed at momentum \mathbf{q}_e is proportional to $I(\mathbf{q}_e) = \phi(\mathbf{q}_e) \phi(\mathbf{q}_e)^*$ with $\mathbf{q}_e = \mathbf{k}_1 + \mathbf{k}_2 - \mathbf{k}_0$, the momentum of the ejected electron *before* the collision [the electron momentum is minus the recoil momentum as defined in Eq. (2)]. Diffraction can be seen as a distortion of the incoming and outgoing waves. With dif-

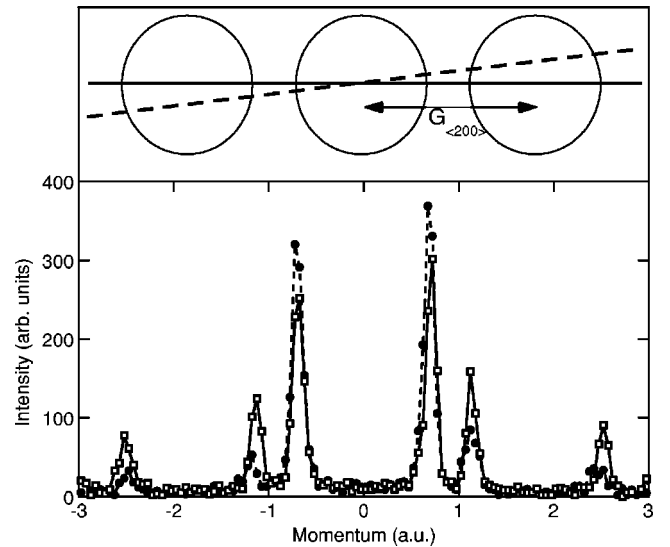


FIG. 9. The effect of alignment on diffraction and peak positions for measurements near the $\langle 1,0,0 \rangle$ alignment. Diffraction effects are largest for the best aligned crystal (open squares). The position of the outer diffracted peaks move slightly inward with increasing misalignment. This is explained in the top inset. Here the cut through the Fermi surface is approximated by a sphere, and the diffracted spheres (spheres centered on the neighboring reciprocal lattice points) are shown as well. Peaks are observed when the measurement line intersects the spheres. The outermost intersection moves slightly to lower momenta for the misaligned (dashed) measurement.

fraction, the intensity is proportional to $I(\mathbf{q}_e) = \sum_{i,j} A_{i,j} \phi(\mathbf{q}_e + \mathbf{G}_i) \phi(\mathbf{q}_e + \mathbf{G}_j)^*$, with $A_{i,j}$ determined by the values of the coefficients $C_{0,1,2}(z)$.

There are two different types of contributions: those with $i=j$ and those with $i \neq j$. The first contribution has a shape similar to that without diffraction, but it is shifted by a reciprocal lattice vector. The second contribution is sensitive to the phase difference between the wave function at $\mathbf{q}_e + \mathbf{G}_i$ and $\mathbf{q}_e + \mathbf{G}_j$, and would have a distribution that is completely different from that without diffraction. For example, near the bottom of the band only a single plane wave is occupied. Thus, the contribution with $i \neq j$ is a product of two terms: $\phi(\mathbf{q}_e + \mathbf{G}_i)$ and $\phi(\mathbf{q}_e + \mathbf{G}_j)^*$. At least one of these two terms is zero and hence these off-diagonal terms do not affect the momentum density at the bottom of the band. These off-diagonal terms are most likely to be important for wave functions with a large density near the Brillouin zone boundary, with either \mathbf{G}_i or \mathbf{G}_j corresponding to $\langle 0,0,0 \rangle$. We have not yet seen an unambiguous sign of these nondiagonal contributions. Hence, we will try to analyze our data assuming that only the first type of contribution occurs.

We consider now two measurements: one with the spectrometer y direction aligned with the $\langle 100 \rangle$ direction, and a measurement of the same crystal with a misalignment of about 5° (the axis of rotation is the surface normal). Looking at the momentum distribution at E_f , as displayed in Fig. 9, one observes a large dependence on the alignment of the high-momentum peaks (near 1.15 and 2.5 a.u.). This indicates that diffraction plays an important role. The best

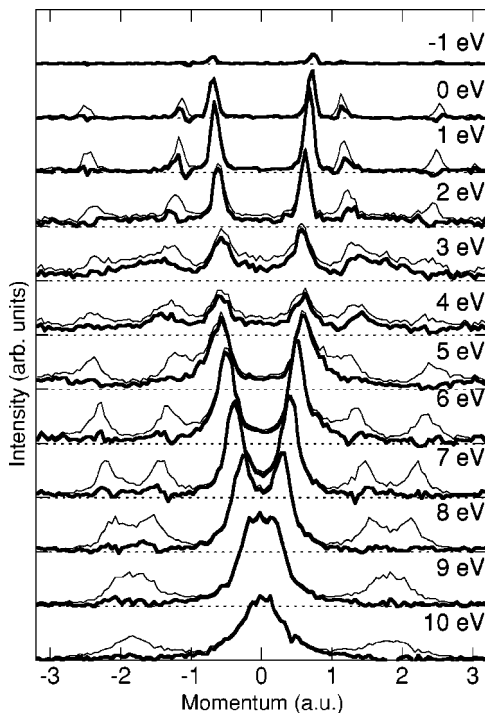


FIG. 10. The momentum profiles on the $\langle 100 \rangle$ binding energies as measured (thin lines), and after removal of the diffracted contribution (thick lines).

aligned spectra showed largest intensity shifted by $\mathbf{G} = \pm(2, 0, 0)$ from the main peaks. For a well aligned sample the diffraction condition $2\mathbf{k}_j \cdot \mathbf{G}_i + G_i^2 = 0$ is fulfilled for $\mathbf{G} = \pm(2, 0, 0)$ for both the incoming and outgoing electrons, as discussed earlier. Thus, it is expected that near perfect alignment, the diffracted peaks reach maximum intensity.

Which part of the peaks at ± 1.15 a.u. is due to diffraction and which part is due to contribution of more than a single plane wave to the Bloch function? This is the question we will now try to answer. For this we plot the momentum profiles for a range of binding energies in Fig. 10 for the measurement well aligned with the $\langle 100 \rangle$ direction. Besides the main dispersing feature, a less intense feature is present both at low and at high momenta, displaying the same (but shifted) dispersing behavior as the main feature. For the momentum distribution near 9 eV binding energy, the three peaks correspond to three Γ points. The theory of the electronic structure of copper predicts that the occupation of the inner valence band approaches zero well before the second Γ point is reached (see Fig. 1). Thus, we assume that all intensity here is due to diffraction. We establish that ratio of the diffracted intensity to the main intensity is $C_{l,r}$ (C_l for the diffracted peak at negative momentum, C_r for that at positive). We now subtract from the measured $I(\mathbf{q} \pm \mathbf{G}, \varepsilon)$ the amount $C_{l,r} I(\mathbf{q}, \varepsilon)$. First, we do this subtraction for $q=0$ as here the main intensity is not expected to be due to diffraction, and subsequently do the subtraction for larger $|q|$ values. The resulting momentum distributions are shown in Fig. 10 as thick lines. This procedure removes all the smaller structures at high momentum values of $|q|$. However, near the Fermi level, part of the contribution at $|q|=1.15$ a.u. re-

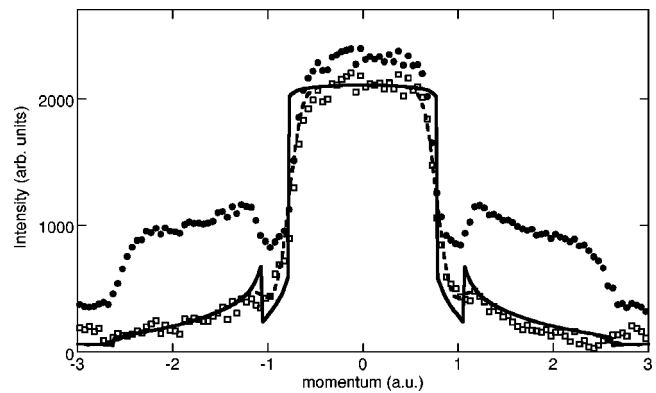


FIG. 11. The momentum density as measured (filled circles), after subtraction of the diffracted peak (open squares). The measurement is compared to the calculated momentum density without any broadening (full line) and with broadening of 0.1 a.u. (dashed line)

mains, whereas the outer peaks near $|q|=2.5$ a.u. have disappeared. Thus, we think that the part of the peak at $|q|=1.15$ a.u. remaining after the subtraction is a measurement of the contribution of $|q|=1.15$ a.u. to the Bloch function.

Integrated over energy these data present the momentum density. In the raw data, intensity extends up to high binding energies, and hence the energy window for the integration is not easily defined. Therefore, we deconvoluted the data first for inelastic energy losses as described in Sec. III E, and then subtracted the diffracted contribution. The results are shown in Fig. 11 and these data are compared to the LMTO calculation. The clarity with which the second break is observed in the calculated distribution depends strongly on the momentum resolution assumed. Using a momentum resolution of 0.1 a.u., a good agreement between calculated and measured data is obtained.

F. Comparison of the multiple scattering corrected data with theory

We demonstrated in the previous sections that we can, at least to the first order, correct the data for inelastic multiple scattering, and for the main elastic multiple scattering (diffraction) contributions. We now can try to put it all together and compare the data corrected for both types of events directly with theory. This is done in Fig. 12 for the $\langle 100 \rangle$ direction. Ideally, a full many-body perturbation calculation would be used to compare with experiment. However, it is computationally too costly to do this at a fine enough grid. Therefore, a FT-LMTO calculation was used, broadened with lifetime broadening, taken from jellium calculations.²⁸ The calculation was done on a fine momentum grid (0.015 a.u.) and subsequently integrated over 0.1 a.u. intervals. This procedure gives significantly better results than calculating at a single momentum value centered at the experimental interval as the integration over the fine grid introduces some effects of finite momentum resolution into the calculation.

The alignment of the measured and calculated peaks (i.e., dispersion) is not perfect, and the observed discrepancies are in line with those shown in Fig. 5. Here we want to discuss

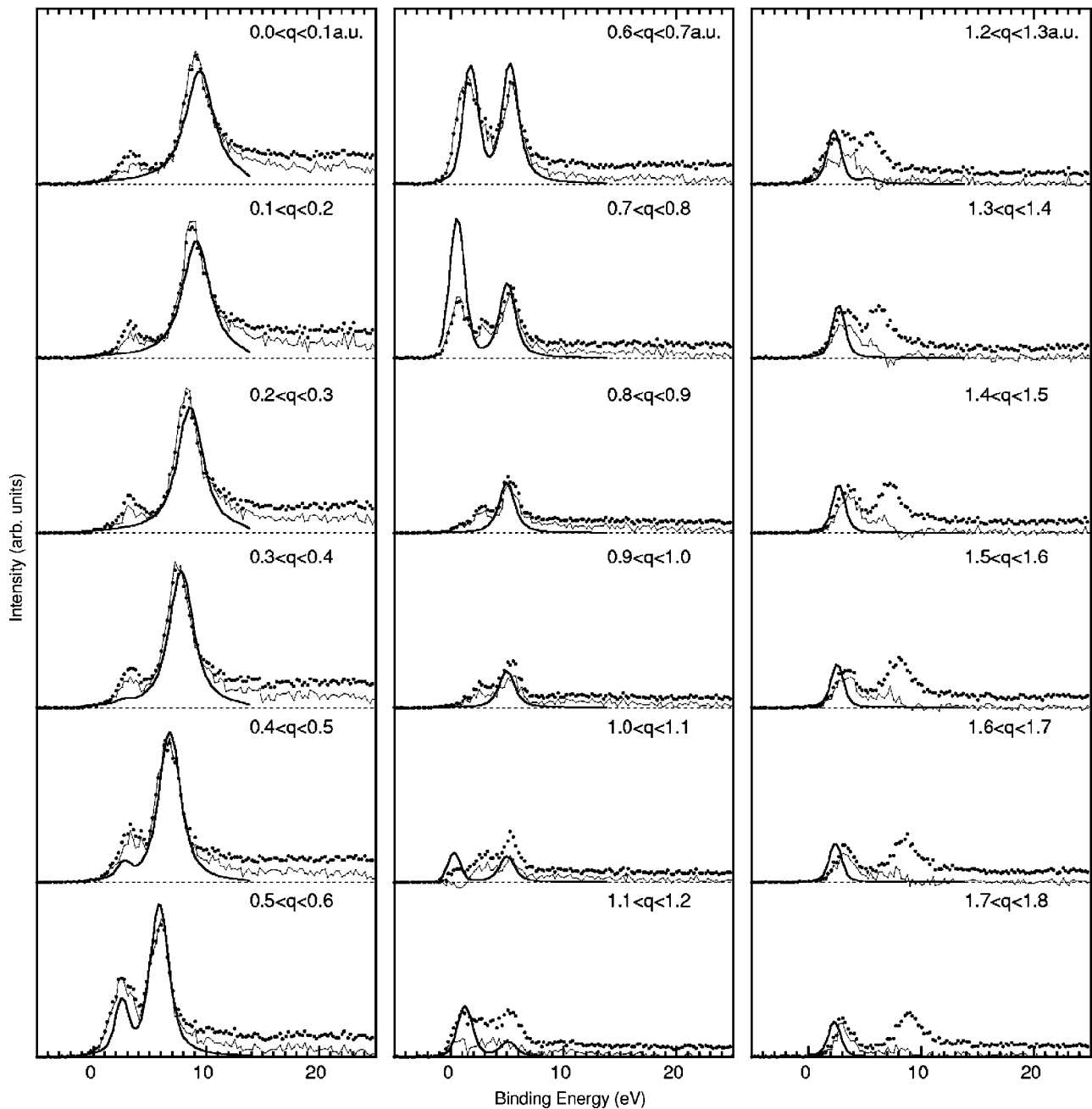


FIG. 12. Energy spectra at the indicated momentum values along the $\langle 100 \rangle$ direction. The raw measured intensity (dots) and after corrections for the inelastic and elastic energy loss processes (thin line) compared to the LMTO theory with additional life-time broadening based on jellium calculations (thick line).

mainly the peak shapes and intensities. Generally, there is a reasonable similarity between the calculated and measured intensities. One of the noticeable exceptions is near k_f ($0.7 < q < 0.8$). Although the $3d$ part of the calculated distribution has the right intensity, the peak height of the sp band is more than twice too high. As the Fermi vector in the calculation corresponds to 0.78 a.u. (slightly more than the de Haas-van Alphen value of 0.76 a.u.) the sp peak is completely absent in the $0.8 < q < 0.9$ bin, whereas in the experiment it still has a small intensity due to finite momentum resolution. However, some smearing out due to finite momentum resolution effects cannot explain the large discrepancy

between experiment and theory in the $0.7 < q < 0.8$ interval.

From many-body perturbation theory of the electron gas, we know that not all the intensity of the spectral function is concentrated in the quasiparticle branch, but that about 30% of the intensity is in a satellite branch, shifted to higher binding energy by about the plasmon energy.²⁹ In the momentum density (energy-integrated spectral function) the quasiparticle branch causes a discontinuity at k_f , whereas the satellite branch reduces in intensity more gradually. Thus, electron correlation effects are expected to reduce the discontinuity in the normalized momentum density at k_f from 1 to ≈ 0.7 .

However, attempts, based on Compton scattering, to measure the discontinuity for metals such as Li have resulted in dramatically lower values (0.1 ± 0.1).³⁰ Our result seems to indicate that the calculated intensity of the quasiparticle peak near k_f could be too large, resulting in a calculated discontinuity that is too large.

Slightly over 1 a.u., the same band (after reaching an extremum at the X point) crosses the Fermi level again. Between 1 and 1.2 a.u., the theory predicts significant intensity in this band. However, in the experiment, after corrections for diffraction the intensity is again significantly smaller. Thus, the main discrepancies between the intensity as predicted by theory and observed in the experiment are close to the Fermi level.

IV. CONCLUSION

Electron momentum spectroscopy has been applied to single-crystal copper. A wide variety of properties can be

measured directly with this technique. Interpretation is very straightforward, and the only complicating factor is multiple scattering. We showed that the inelastic scattering effects can be deconvoluted out quite well, using the measured energy loss spectrum, and that a large part of the elastic scattering effects (diffraction) can be corrected for. After making these corrections, the measured intensity distribution shows good agreement with the calculated spectral function. Near the Fermi level there are some significant discrepancies between theory and experiment, the main one being that the calculated sp density is much higher than observed.

ACKNOWLEDGMENT

We acknowledge financial support of the Australian Research Council.

*E-mail: Maarten.Vos@anu.edu.au

- ¹A. S. Joseph, A. C. Thorsen, E. Gertner, and L. E. Valby, *Phys. Rev.* **148**, 569 (1966).
- ²R. Courths and S. Hüfner, *Phys. Rep.* **112**, 53 (1984).
- ³S. Berko, *Positron Solid State Physics* (North Holland Publ., 1983), pp. 64–145.
- ⁴H. Kondo, T. Kubota, H. Nakashima, Y. Murakami, and S. Tanigawa, *Phys. Status Solidi B* **177**, 345 (1993).
- ⁵J. Dumond, *Rev. Mod. Phys.* **5**, 1 (1933).
- ⁶Y. Sakurai, S. Kaprzyk, A. Bansil, Y. Tanaka, G. Stutz, H. Kawata, and N. Shiotani, *J. Phys. Chem. Solids* **60**, 905 (1999).
- ⁷Y. Kubo, Y. Sakurai, and N. Shiotani, *J. Phys.: Condens. Matter* **11**, 1683 (1999).
- ⁸O. Jepsen, D. Glötzel, and A. R. Mackintosh, *Phys. Rev. B* **23**, 2684 (1981).
- ⁹A. H. MacDonald, J. M. Daams, S. H. Vosko, and D. D. Koelling, *Phys. Rev. B* **25**, 713 (1982).
- ¹⁰V. N. Strocov, R. Claessen, F. Aryasetiawan, P. Blaha, and P. O. Nilsson, *Phys. Rev. B* **66**, 195104 (2002).
- ¹¹A. Marini, G. Onida, and R. Del Sole, *Phys. Rev. Lett.* **88**, 016403 (2002).
- ¹²A. Yamasaki and T. Fujiwara, *J. Phys. Soc. Jpn.* **72**, 607 (2003).
- ¹³I. E. McCarthy and E. Weigold, *Rep. Prog. Phys.* **51**, 299 (1988).
- ¹⁴A. S. Kheifets, D. R. Lun, and S. Y. Savrasov, *J. Phys.: Condens. Matter* **11**, 6779 (1999).
- ¹⁵X. Guo, Z. Fang, A. S. Kheifets, S. A. Canney, M. Vos, I. E. McCarthy, and E. Weigold, *Phys. Rev. B* **57**, 6333 (1998).

- ¹⁶M. Vos, G. P. Cornish, and E. Weigold, *Rev. Sci. Instrum.* **71**, 3831 (2000).
- ¹⁷M. Vos and E. Weigold, *J. Electron Spectrosc. Relat. Phenom.* **112**, 93 (2000).
- ¹⁸M. Vos, V. A. Sashin, C. Bowles, A. S. Kheifets, and E. Weigold, *J. Phys. Chem. Solids* (to be published).
- ¹⁹M. Vos, A. S. Kheifets, V. A. Sashin, and E. Weigold, *J. Phys. Chem. Solids* **64**, 2507 (2003).
- ²⁰M. Vos, A. S. Kheifets, V. A. Sashin, E. Weigold, M. Usuda, and F. Aryasetiawan, *Phys. Rev. B* **66**, 155414 (2002).
- ²¹S. Å. Lindgren, J. Paul, and L. Walldén, *Solid State Commun.* **44**, 639 (1982).
- ²²V. N. Strocov *et al.*, *Phys. Rev. Lett.* **81**, 4943 (1998).
- ²³M. B. Nielsen, Z. Li, S. Lizzit, A. Goldoni, and P. Hofmann, *J. Phys.: Condens. Matter* **15**, 6919 (2003).
- ²⁴S. Tougaard, *Phys. Rev. B* **34**, 6779 (1986).
- ²⁵F. Aryasetiawan, L. Hedin, and K. Karlsson, *Phys. Rev. Lett.* **77**, 2268 (1996).
- ²⁶L. J. Allen, I. E. McCarthy, V. W. Maslen, and C. J. Rossouw, *Aust. J. Phys.* **43**, 453 (1990).
- ²⁷Z. Fang, R. S. Matthews, S. Utteridge, M. Vos, S. A. Canney, X. Guo, I. E. McCarthy, and E. Weigold, *Phys. Rev. B* **57**, 12 882 (1998).
- ²⁸L. Hedin, *Phys. Rev.* **139**, A796 (1965).
- ²⁹L. Hedin and S. Lundqvist, *Solid State Phys.* **23**, 1 (1969).
- ³⁰W. Schülke, G. Stutz, F. Wohlert, and A. Kaprolat, *Phys. Rev. B* **54**, 14 381 (1996).